Cancer Letters 507 (2021) 26–38

Contents lists available at ScienceDirect

Cancer Letters

journal homepage: www.elsevier.com/locate/canlet

Endogenous retrovirus expression activates type-I interferon signaling in an experimental mouse model of mesothelioma development

Suna Sun [a], Francesca Frontini [a], Weihong Qi [b], Ananya Hariharan [a], Manuel Ronner [a], Martin Wipplinger [a], Christophe Blanquart [c], Hubert Rehrauer [b], Jean-François Fonteneau [c], Emanuela Felley-Bosco [a,*]

[a] Laboratory of Molecular Oncology, Department of Thoracic Surgery, Lungen- und Thoraxonkologie Zentrum, University Hospital Zurich, Sternwartstrasse 14, 8091, Zurich, Switzerland
[b] Functional Genomics Center Zürich, ETH Zürich/University of Zürich, Zürich, Switzerland
[c] Université de Nantes, CNRS, INSERM, CRCINA, F-44000, Nantes, France

ARTICLE INFO

Keywords:
Mesothelioma
Endogenous retrovirus
Type-I interferon Signaling

ABSTRACT

Early events in an experimental model of mesothelioma development include increased levels of editing in double-stranded RNA (dsRNA). We hypothesised that expression of endogenous retroviruses (ERV) contributes to dsRNA formation and type-I interferon signaling. ERV and interferon stimulated genes (ISGs) expression were significantly higher in tumor compared to non-tumor samples. 12 tumor specific ERV ("MesoERV1-12") were identified and verified by qPCR in mouse tissues. "MesoERV1-12" expression was lower in mouse embryonic fibroblasts (MEF) compared to mesothelioma cells. "MesoERV1-12" levels were significantly increased by demethylating agent 5-Aza-2′-deoxycytidine treatment and were accompanied by increased levels of dsRNA and ISGs. Basal ISGs expression was higher in mesothelioma cells compared to MEF and was significantly decreased by JAK inhibitor Ruxolitinib, by blocking Ifnar1 and by silencing Mavs. "MesoERV7" promoter was demethylated in asbestos-exposed compared to sham mice tissue as well as in mesothelioma cells and MEF upon 5-Aza-CdR treatment.

These observations uncover novel aspects of asbestos-induced mesothelioma whereby ERV expression increases due to promoter demethylation and is paralleled by increased levels of dsRNA and activation of type-I IFN signaling. These features are important for early diagnosis and therapy.

1. Introduction

Malignant mesothelioma (reviewed in Ref. [1]) is a rapidly fatal and highly resilient tumour arising in the thin layer of tissue known as the mesothelium, which has mesodermal origins and covers many of the important internal organs like the lungs (pleural mesothelioma), peritoneal cavities (peritoneal mesothelioma), the sacs surrounding the heart (pericardial mesothelioma) and the testis (tunica vaginalis mesothelioma). Although mesothelioma is a rare cancer, its incidence is still rising; hence research aimed at better understanding of the biology of the disease is still necessary, because it may help in novel therapeutic approaches. Some aspects, such as resistance to oncolytic therapy due to constitutive activation of type-I interferon (IFN) pathway in tumor [2], are of special interest in the era of immunotherapy implementation also in this cancer type (reviewed in Ref. [3]).

Mesothelioma is the sixth of 31 cancer types with most prevalent 38-interferon stimulated genes (ISGs) signature [4] and, in a large fraction of ISG-high tumors, no immune cells, possibly contributing to the phenotype, have been detected, indicating spontaneous IFN production by cancer cells *per se*. This is consistent with a recent study that has shown that primary mesothelioma cells maintain the activation of the type-I IFN signaling pathway [5]. Importantly, in the context of mesothelioma, type-I IFN signature is linked to both, clinical outcome and specific driver mutations [6]. A recent large-scale study has comprehensively characterized most genetic alterations and four distinct molecular profiles in malignant pleural mesothelioma, which have been called epithelioid (which actually include mostly only pure epithelioid histotype), biphasic-epithelioid, biphasic-sarcomatoid and sarcomatoid [7]. It extends the histopathological classification separating epithelioid, sarcomatoid and biphasic of mesothelioma (reviewed in Ref. [1]). Based on the mRNA expression profile, tumors are clustered into four

* Corresponding author.
E-mail address: emanuela.felley-bosco@usz.ch (E. Felley-Bosco).

https://doi.org/10.1016/j.canlet.2021.03.004
Received 4 November 2020; Received in revised form 23 February 2021; Accepted 3 March 2021
Available online 10 March 2021

Abbreviations

5-Aza-CdR	5-Aza-2′-deoxycytidine
ADAR	adenosine deaminase acting on RNA
BAP1	BRCA1-associated protein
Ddx58	DEAD (Asp-GluAla-Asp) box polypeptide 58
DNMT	DNA-Methyl transferase
dsRNA	double stranded RNA
EVE	Endogenous Viral Elements
ERV	endogenous retroviruses
FFPE	formalin-fixed, paraffin-embedded
gDNA	genomic DNA
Ifitm1	interferon induced transmembrane protein 1
IFN	interferon
Ifnβ1	type-I interferon beta
Ifnar1	IFN-α/β receptor 1
ISGs	interferon stimulated genes
LTR	long terminal repeat
MEF	mouse embryonic fibroblasts
"M"	Methylated
Mavs	mitochondrial antiviral signaling protein
MV	Measle Virus
ORF	open reading frames
qMSP	quantitative methylation specific PCR
RNA-seq	RNA sequencing
RT-qPCR	real-time quantitative PCR
SINE	short-interspersed nuclear elements
TCGA	The Cancer Genome Atlas
TE	transposable elements
TET	ten-eleven translocations
"U"	unmethylated

groups in a parallel study performed by The Cancer Genome Atlas (TCGA) consortium [6]. Pathway enriched analysis of genes expressed in the clusters revealed, among others, enrichment of reactome antiviral mechanism by ISGs in one of the clusters, and this is confirmed in the epithelioid group of Bueno et al. [7]. Patients with this profile have a better clinical outcome [8].

We recently observed in an experimental animal model of asbestos-induced mesothelioma development [9], that exposure to crocidolite (blue asbestos) increased the levels of RNA mutations and the most abundant changes were A to G mutations, likely resulting from hydrolytic deamination of adenosine downstream of adenosine-deaminase acting on double strand (ds)RNA (Adar) activity [10]. Adenosine deamination produces inosine, which is detected as guanosine in RNA-sequencing (RNA-seq). dsRNAs, like other nucleic acids, are part of the signals recognized by patterns recognition receptor family which are able to activate innate immunity via the production of type-I IFN [11]. The enzymes carrying out adenosines deamination destabilize dsRNA structures, thereby acting as negative feedback regulators. The nature of the edited endogenous dsRNA has been investigated in several studies (reviewed in Ref. [12]). In mouse normal monocytes or tissues, 32–73% of all editing events occurs in short-interspersed nuclear elements (SINE) and 9–27% in long terminal repeat (LTR)-retrotransposons while in human normal monocytes or tissues, 43–96% of all editing events occurs in SINE and 2.4–7.4% in LTR-retrotransposons depending on the type of cells or tissue analyzed. LTR-retrotransposons include endogenous retroviruses (ERV) (reviewed in Ref. [12]). ERVs are remnants of exogenous retrovirus insertions into the germline and contain deteriorating retroviral protein open reading frames (ORF), flanked by transcription-promoting LTRs [13]. Altogether, SINE and LTR-retrotransposons regions cover 42% and 37% of the genome in human and mice, respectively. Taking into account that 70% of the genome is transcribed and only 2% of the genome encodes for proteins, this may explain the reason why the vast majority of editing sites in human and primates are in inverted repeat SINE (Alu elements in human) and ERV which forms stable dsRNA structures, and are largely in non-coding regions of the genome (reviewed in Ref. [12]). The abundancy of the targets render them attractive to investigate because it may result in increased sensitivity.

The aim of this study was to investigate whether in asbestos-induced mesothelioma there is an increased expression of certain ERV able to form dsRNA structure that contribute to stimulating type-I IFN signature.

2. Materials and methods

2.1. Cell culture, drug or blocking antibodies treatments, and RNA interference

MEF (Sigma Aldrich or kind gift of W. Krek, ETHZ) were cultured in DMEM/F12 supplemented with 10% FCS, 1% L-Glutamine and 1% penicillin/streptomycin. RN5 mesothelioma [9,14], AK7 (initially generated by Kane [15], kind gift of Prof. Jean Bignon, CHU Henri Mondor, Créteil, France) and AB1 ([16] kind gift of Dr. Luc Willem, University of Liège) cells were cultured in MPM medium (DMEM/F12 supplemented with 15% FCS, 0.4 μg/ml hydrocortisone, 10 ng/ml EGF, 1% L-Glutamine, 1% penicillin/streptomycin, 1% ITS, 100 μM β-MercaptoEtOH, 1 mM Pyruvate). All cell lines were cultured in a humidified incubator (at 37 °C with 5% CO2), passaged every 2–4 days. Cells were seeded in 6-well plates and after 24 h were treated with 25 nM 5-Aza-2′-deoxycytidine (5-Aza-CdR) (Selleckchem, Cat No.S1200), 1 μM Ruxolitinib (Selleckchem, Cat No.S1378) or DMSO as mock. To determine response to type-I IFN, cells were exposed to 60U/ml Recombinant Mouse IFN-beta Protein (R&D Systems (biotechne), Cat No. 8234-MB) for 24 h. Blocking IFN-α/β receptor 1 (Ifnar1) was achieved using anti IFN-aR1 (10 μg/ml, MAR1-5A3 antibodies, sc-53591L, RRID: AB_783928) and comparing to mouse isotype control (10 μg/ml, Cat.# MABF1081Z, Mouse IgG1-k Negative control, clone MOPC-21, RRID: AB_2828024).

In order to down-regulate mitochondrial antiviral signaling protein (Mavs) expression, ON-TARGETplus SMARTpool siRNAs against *Mavs* or siGENOME Non-Targeting siRNA pool #2 and DharmaFECT 1 transfection reagent were obtained from Dharmacon. siRNA dissolved in 1X siRNA buffer (Dharmacon) was combined with transfection reagent dissolved in OptiMEM (final concentration 0.084%) and incubated for 20 min. Then, cells resuspended in normal growth medium were added to the siRNA/DharmaFECT 1 mixture and seeded onto plates, allowing for a final siRNA concentration of 10 nM. 0.8×10^5 cells (12-well plate) were plated for whole cell protein lysates as wells as RNA extraction 72 h later.

2.2. RNA extraction, cDNA synthesis and RT-qPCR

0.5 μg of total RNA was extracted from cells using RNeasy isolation kit (QIAGEN, Cat No.74106) and reverse-transcribed using the Quantitect Reverse Transcription Kit (QIAGEN, Cat No.205311) according to the manufacturer's instructions.

Synthesized cDNA was diluted 1:60 and used for real-time quantitative PCR (RT-qPCR). SYBR green (Thermo Fisher, Cat No.4367659) and gene specific primers (sequences listed in Additional file1: Table S1)

were used for PCR amplification and detection on a 7500 FAST Real-Time PCR System (Applied Biosystems, Thermo Fisher Scientific) or QuantStudio 5 Real-Time PCR System. Relative mRNA levels were determined by comparing the PCR cycle thresholds between cDNA of a specific gene and beta actin or Tubulin Beta 4A Class IVa (ΔCt).

2.3. DsRNA digestion by RNase III

Purified 5 μg total RNA from RN5 cells was subjected to digestion with 0.2 U RNase III (AMBION, Cat.No.AM2290) in a total volume of 50 μL at 37 °C for 10 min according to the manufacturer's instructions. Afterwards, 50 μg/ml proteinase K in 10 mM Tris·Cl (pH 7.8)/0.5% SDS was added to the sample to terminate the RNase III digestion and incubated 10 min at 56 °C. RNA was subsequently purified using the Qiazol and miRNeasy mini kit (QIAGEN Cat No. 217004) according the manufacturer's instructions.

2.4. DsRNA pull-down

8 μg of purified RNA was added to 200 μl freshly prepared IP buffer (50 mM Tris-HCl pH 8, 150 mM NaCl, 1% Triton X-100, and 1 mM EDTA), supplemented with 20 U/ml RNase inhibitor. Pre-clearing of the unspecific binding was done by incubating the 8 μg RNA in IP buffer with 20 μl Protein A Sepharose (Bio Vision Cat.No.6501–5) for 30 min at 4 °C on a rotating wheel. After centrifugation (14,000 g at 4 °C for 5 min), 95 ng RNA was taken from the supernatant to determine input. The remaining supernatant was then equally divided into two parts, one for the anti-dsRNA antibody J2 (SCICONS, clone J2, No.10010200, RRID:AB_2651015) and the other for the IgG control of the same isotype. 1 μg of J2 or IgG antibody was added into the supernatant, followed by incubation overnight on a rotating wheel at 4 °C. 10 μl of μl Protein A Sepharose was then added into each reaction, followed by incubation for another 3 h at 4 °C. Next, the beads were collected and washed with 800 μl pre-chilled washing buffer (50 mM Tris-Cl, pH 7.5, 150 mM NaCl) for 5 times. Finally, the co-precipitated RNA on the beads were purified using Qiazol and miRNeasy kit as above.

2.5. DsRNA analysis by J2 staining and flow-cytometry

25×10^3 MEF and 30×10^3 RN5 cells were seeded in 6-well plates on day one, treated with 5-Aza-CdR on day 2 and were collected on day 4 (RN5) or day 7 (MEF). During collection, cells in culture with or without 5-Aza-CdR treatment were trypsinized, washed with PBS and fixed with 4% formaldehyde diluted in PBS for 10 min at room temperature. Cells were permeabilized with 0.1% Saponin, 0.1% BSA in PBS for 30 min. Primary antibodies (anti-dsRNA (J2)) or normal mouse IgG2a (Iso) (Abcam, Cat No. Ab18414) were diluted 1:40 in 0.1% Saponin/PBS and incubated with the cells for 30 min in the dark on ice. Secondary Goat anti-Mouse IgG (H + L) conjugated with Alexa Fluor 488 (Thermo Fisher, Cat No.A11001) were diluted 1:200 in 0.1% Saponin/PBS and incubated with the cells for 30 min on ice. Cells were washed twice with 0.1% Saponin/PBS and were then ready for measurement. Data were acquired with a FACS Attune flow cytometer. Data were analyzed in Attune Cytometric Software.

2.6. Protein extraction, cell fractionation and Western blotting

Total protein extracts were obtained by lysing the cells with hot Laemmli buffer (60 mM Tris-HCl pH 6.8, 100 mM DTT, 5% glycerol, 1.7% SDS) and passed through syringes (26G) [17]. A total of 5 μg protein extract was separated on denaturing 15% SDS-PAGE gels and proteins were transferred onto PVDF membranes (0.45 μm, PerkinElmer, Waltham, MA). Membranes were probed with the following primary antibodies: rabbit anti-phospho-Irf3 (Ser396, D6O1M, CST #29047, RRID:AB_2773013), rabbit anti-Irf3 (D83B9, CST #4302, RRID:AB_1904036), rabbit anti-Ifitm1 (NovusBio NBP1-77171, RRID: AB_11010388), rabbit anti-Rig-I (D14G6, CST#3743 RRID: AB_2269233), mouse anti-Mavs (C-1, Santa Cruz sc-365333 RRID:AB_10844335), and mouse anti-β-actin (C4, MP Biomedicals MP691002 RRID:AB_2335127). Membranes were then incubated with one of the following secondary antibodies: rabbit anti-mouse IgG-HRP (no. A9004) or goat anti-rabbit IgG-HRP (no. A0545), obtained from Sigma Aldrich. The signals were detected by enhanced chemiluminescence (Clarity TM ECL Substrate, BioRad, Hercules, CA) using Fusion Digital Imager (Vilber Lourmat, Marne-la-Vallée, France). Quantification was done using ImageJ software.

Cytosolic and nuclear protein extracts were isolated from RN5 cells as previously described [18] using the NE-PERTM Nuclear and Cytoplasmic Extraction Kit (78833, Pierce Biotechnology) according to manufacturer's instructions and nuclear vs cytosolic purity controls were assessed by probing with anti-PARP (Cell Signaling #9542, RRID: AB_2160739) and with anti-tubulin (Santa-Cruz sc-8035 RRID: AB_628408) antibodies, respectively.

2.7. Genomic DNA extraction from cells and mice tissues

Genomic DNA (gDNA) was extracted from 0.5 to 1 Mio MEF and RN5 cells using the DNeasy Blood&tissue kit (QIAGEN, CAT No.69504) according to manufacturer's instructions.

The tissue used for analysis has been described in our previous study where mice had been exposed to sham or crocidolite (blue asbestos) [9]. Briefly, B6;129S2-Nf2^{tm1Tyj}/J mice backcrossed for ≥ 6 generations on a C57Bl/6J genetic background were exposed to crocidolite asbestos (400 μg/mouse) or with saline (sham) every 3 weeks for a total of eight rounds (i.e. a total of 3.2 mg of crocidolite per mouse). Mice were sacrificed 33 weeks after the first crocidolite injection.

gDNA extraction from formalin-fixed, paraffin-embedded (FFPE) tissues from sham or crocidolite exposed mice was performed as follows: defined area of tissues (mesothelium, tumor) were scratched from slides (thickness ~ 20 μm, diameter ~ 2 mm) using #10 blade and transferred into a 2 ml tube. 1 ml xylene was added to dissolve the paraffin, and then washed 3 times with 100% EtOH. Tissue was resuspended in 180 μl ATL Buffer followed by addition of 20 μl proteinase K and incubation at 56 °C, 450 rpm, until the tissue was completely lysed. Then 180 μl ATL Buffer + 20 μl proteinase K were added again followed by another 5–10 min incubation at 56 °C. After vigorous vortexing to homogenize the mixture 800 μg RNase A were added and incubated for 2 min at room temperature. Afterwards, gDNA was extracted using the "DNeasy Blood & Tissue" kit (QIAGEN, Cat No.69504) according to manufacturer's instructions. Due to limited availability of samples all crocidolite (tumor and inflamed mesothelium) were pooled and compared to samples from sham treated mice.

2.8. Bisulfite treatment for gDNA and qMSP

To perform methylation studies, gDNA was subjected to sodium bisulfite treatment performed using the EZ DNA Methylation Gold™ Kit (Zymo Research, Cat No. D5005 & D5006) according to manufacturer's instructions, with an extra step of incubating the samples for 7 min at 95C before adding CT Conversion Reagent solution. Measurement was performed by quantitative methylation specific PCR (qMSP). Methylated ("M") - and unmethylated ("U")-specific primers (Additional file1: Table S1) were designed within CpG islands surrounding the promoter of "MesoERV7″ by using the online platform MethPrimer [19] as per standard qMSP design guidelines. Commercial methylated mouse DNA (ZYMO RESEARCH, Cat No.D5012) was used to generate absolute methylation standard curve by performing bisulfite conversion and qMSP with "M" primers. Use of "U" primers on serially diluted demethylated DNA resulted in a curve parallel to methylation standard curve. The copy number of methylated and unmethylated sequences for "MesoERV7" promoter were both established by extrapolation from the standard curve. The percentage of methylation was defined as the ratio

between methylated molecules and the sum of methylated and unmethylated molecules [20]. End point PCR products were run on a 4% agarose gel and visualized under UV 365 nM (VILBER LOURMAT, serial No.13200087). Sequencing confirmed that the "M" primers recognized a fully methylated product, while the "U" primers recognized a fully demethylated product in gDNA from mesothelioma cells.

2.9. Methods for computing the A to G index

As previously described, mice were repeatedly injected intraperitoneally over a time course of 21 weeks with crocidolite or sham-exposed and sacrificed at 33 weeks, 12 weeks after the last crocidolite exposure [9]. Tissues, among which mesothelium and tumor masses, were collected from euthanized mice and consecutively processed for RNA-seq analysis. The mice sacrificed corresponded to three groups: sham, crocidolite-exposed mice with pre-neoplastic lesions, and crocidolite-exposed mice bearing tumors. The RNA isolation, library generation, and RNA-seq analysis pipelines are previously described [9]. RNA-seq data are deposited in the European Nucleotide Archive, accession no PRJEB15230. RNA-seq reads were pre-processed using fastp (0.20.0). Sequencing adapters and low quality ends (averaged quality lower than 20 in a sliding window of 4 bp) were trimmed. Trimmed reads with average quality above 20 and length longer than 50 bp were aligned to the mouse reference genome (UCSC mm10) using STAR (2.7.3a) with one pass mode. PCR duplicates were marked using Picard (2.18.0). Primary alignments were extracted using samtools (1.3.1) and were used for computing the A to G index by applying the python package RNAEditingIndexer (https://github.com/a2iEditing/RNAEditingIndexer).

2.10. ERV analysis

For analysis of transposable elements (TE) expression, TEtranscripts [21] was used to obtain TE counts and perform differential expression analysis using DESeq2. TE loci were considered to be significantly differentially expressed when the adjusted p-values were <0.01, and where the log2 of the fold change was >1 for upregulated loci and < -1 for downregulated loci. ERV sequences were downloaded from Endogenous Viral Elements (EVE) database (http://geve.med.u-tokai.ac.jp/download/). The gEVE database has ORF and metORF sequences. ORF sequences correspond to nucleotide or amino acid sequence that may not start with an ATG codon (nucleotide) or Methionine (amino acid), respectively. Their expression in RNA-seq data [9] was quantified using featureCounts in the Bioconductor package Rsubreads.

2.11. Immunohistochemistry

Immunohistochemistry was performed as previously described [9] using rabbit anti-Stat1 (Cell Signaling Technology Cat# 9172, RRID: AB_2198300) antibodies. Primary antibody was omitted in control.

2.12. Statistical analysis

The figures represent the mean values from at least three independent experiments. Paired and unpaired *t*-test, Mann–Whitney, Kruskal Wallis or one-way ANOVA tests were used and have been specified when used. Error bars indicate the standard error of the mean. Statistical analysis was performed using Prism 8 (Graphpad 8.0.0).

3. Results

3.1. RNA editing activity and ERV expression increases upon mesothelioma development

In our previous study [9] mesothelioma development was investigated in mice which were repeatedly injected with crocidolite or sham intra-peritoneally over a time course of 21 weeks. Mice were sacrificed at 33 weeks, 12 weeks after the last crocidolite exposure, to collect mesothelium and mesothelioma tissue for RNA-seq analysis. The sacrificed mice corresponded to three groups: sham, crocidolite-exposed mice with pre-neoplastic lesions, and crocidolite-exposed mice bearing tumors (Fig. 1A). We revisited our RNA-seq data [9] using a genome wide quantification tool of adenosine to inosine editing activity that has been recently developed [22]. This computational tool allows computing an index weighting A-to-G mismatches by the number of all adenosines covered in mouse SINE B1 (equivalent of human Alu) and SINE B2. While the A to G index in the tissue of sham mice is within the range recently described [22], we observed a significant increase in crocidolite exposed groups (Fig. 1B). Subsequently, we analyzed the nucleotides enriched or underrepresented around editing sites and we observed (Fig. 1C) that the sequence-motif is consistent with the ADAR-dependent editing signature with the nucleotides at the 5′ and 3′ to the edited A (-1 and $+1$ position) having a strong preference for G depletion and enrichment, respectively [23] and an enrichment of T (U in RNA) at the 5' position [24], validating the role of RNA deamination in this process.

Although the A to G index is based on SINE B1 and B2 analysis because they are representative of RNA editing activity [22], other dsRNA structures originating from transposable elements (TE), highly represented sequences in the genome, are known to be edited [10, 24–26]. We employed our RNA-sequencing data to determine which TE subfamilies are differentially expressed during mesothelioma development using TEtranscripts [21]. We observed that LTR represent the most abundant TE upregulated and downregulated during mesothelioma development (Fig. 1D). Within LTR, ERV1 and ERVK families have the highest number of upregulated loci (Fig. 1E, Additional file1: Table S2) while L1 and TcMar-Tigger were the most upregulated families in LINE1 and DNA transposons, respectively, in tumors (Additional file2: Fig. S1). ERV expression upon treatment with DNA methyltranferase (DNMT) inhibitors has been described to trigger type-I IFN signaling through generation of dsRNA [27] and ERV sequences have been co-opted in driving the evolution of gene-regulatory networks involved in innate immune response [28]. Tumor samples have a significantly higher number of reads that map to ERV sequences (Fig. 1F and Additional file1: Table S3).

In order to verify the ERV expression, we selected six ERV sequences based on their overall abundancy in tumor (>5000 counts) and their enrichment in crocidolite exposed mice compared to sham controls. One ERV sequence, named by "MuLV_pol_U92", where counts did not differ between crocidolite exposed and sham control mice, was also selected as control (Fig. 2A). Within the mesothelioma enriched ERV sequences, we observed that four of them shared 90 bp, which are located in twenty-one genomic regions, but only twelve are expressed in mouse mesothelioma samples (Fig. 2B and Additional file1: Table S4). We defined these sequences "MesoERV1-12". They belong to the ERV1 family. Both "MesoERV1-12" and "MuLV_pol_U92" were used to design q-PCR primers to validate the selection (Fig. 2C).

Then we tested the basal "MesoERV1-12" and "MuLV_pol_U92" expression in Mouse Embryonic Fibroblasts (MEF), and in mouse mesothelioma RN5 and AK7 (C57BL/6 genetic background, like RN5) cells, used as surrogate for normal tissue versus mesothelioma, respectively. We found that the "MesoERV1-12" expression in mesothelioma cells is significantly higher than in MEF, but there is no difference between MEF and mesothelioma cells for "MuLV_pol_U92" expression, supporting the correlation between "MesoERV1-12" activation and mesothelioma development (Fig. 2D). High levels of expression of "MesoERV1-12" was also observed in AB1 (BALB/c genetic background) mesothelioma cells (Additional file2: Fig. S2), reinforcing the concept of increased ERV expression in mesothelioma. Reasons for differences of expression levels between different strains may include known spontaneous germline mutations due to transposable elements [29], which is supported also by differences in "MuLV_pol_U92" between the different strains.

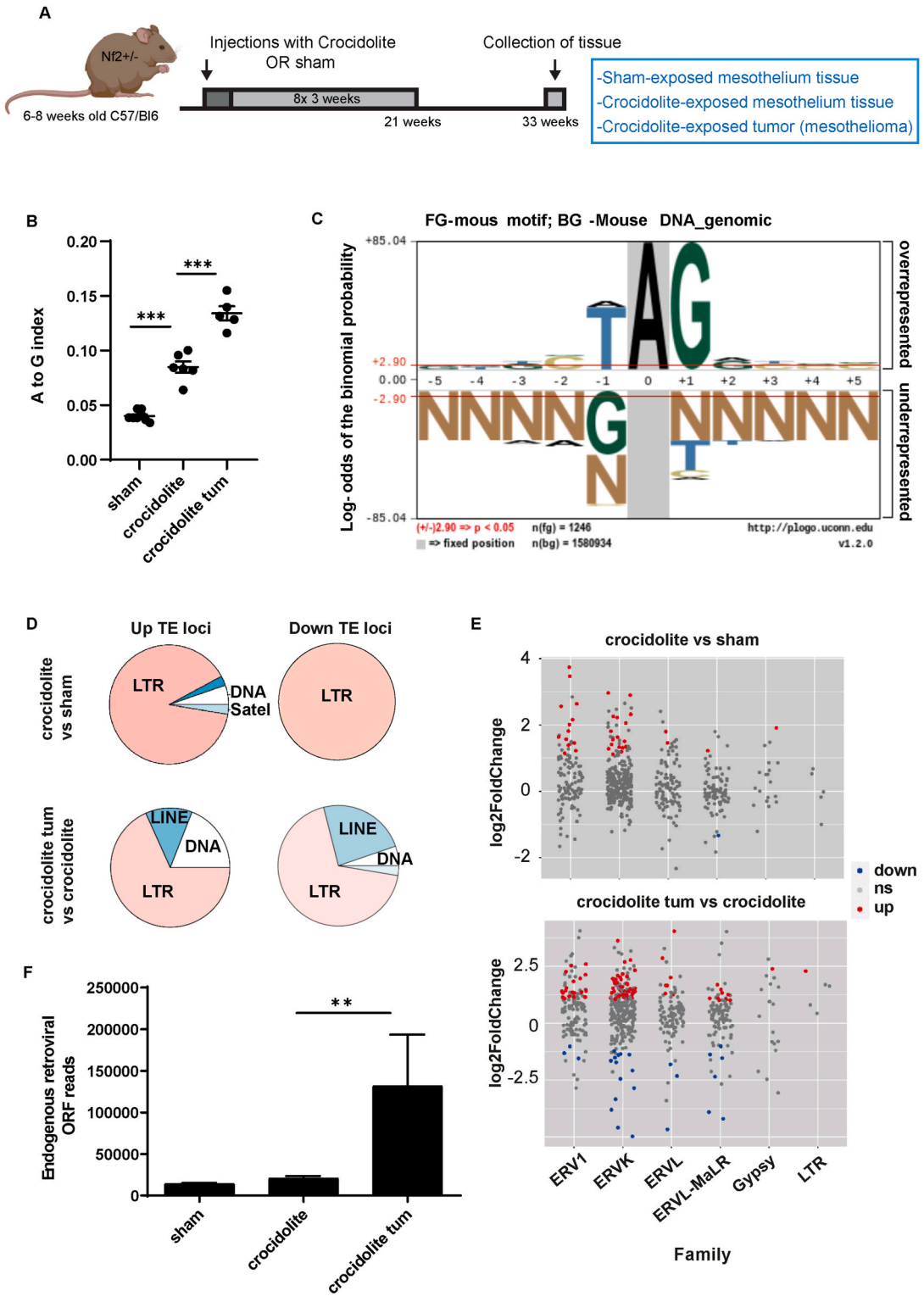

Fig. 1. Increase in levels of RNA editing and endogenous retroviral sequences (ERV) expression during mesothelioma development. (A) Experimental scheme for mouse model of mesothelioma development: 6–8-week-old C57Bl/6J mice were exposed to crocidolite i.p. (400 μg/mouse) every 3 weeks with 8 treatments in total. Thirty-three weeks after initial exposure to crocidolite mice were sacrificed to collect tissues and tumor tissue [9]. (B) A to G index, which reflects ADAR-dependent RNA editing activity, increases in crocidolite (blue asbestos) exposed mice experimental model (***) $P < 0.001$, Mann-Whitney test. (C) Nucleotides enriched close to editing sites. The height of the nucleotide indicates either the degree of overrepresentation (above the line) or the degree of underrepresentation (below the line). (D) Pie charts showing upregulated vs downregulated transposable elements (TEs) loci. (E) LTR loci up or downregulated in crocidolite vs sham or crocidolite tumor vs crocidolite. Significance was defined by padj < 0.01 and abs (log2Fold changes) > 1. Results are shown for loci within the stated LTR families. Ns = expression not significantly changed (F) Expression of ERV sequences increases in tumors induced by crocidolite (ORF: correspond to nucleotide or amino acid sequence that may not start with an ATG codon (nucleotide) or methionine (amino acid)) (**) $P < 0.01$, Mann-Whitney test. (For interpretation of the references to colour in this figure legend, the reader is referred to the Web version of this article.)

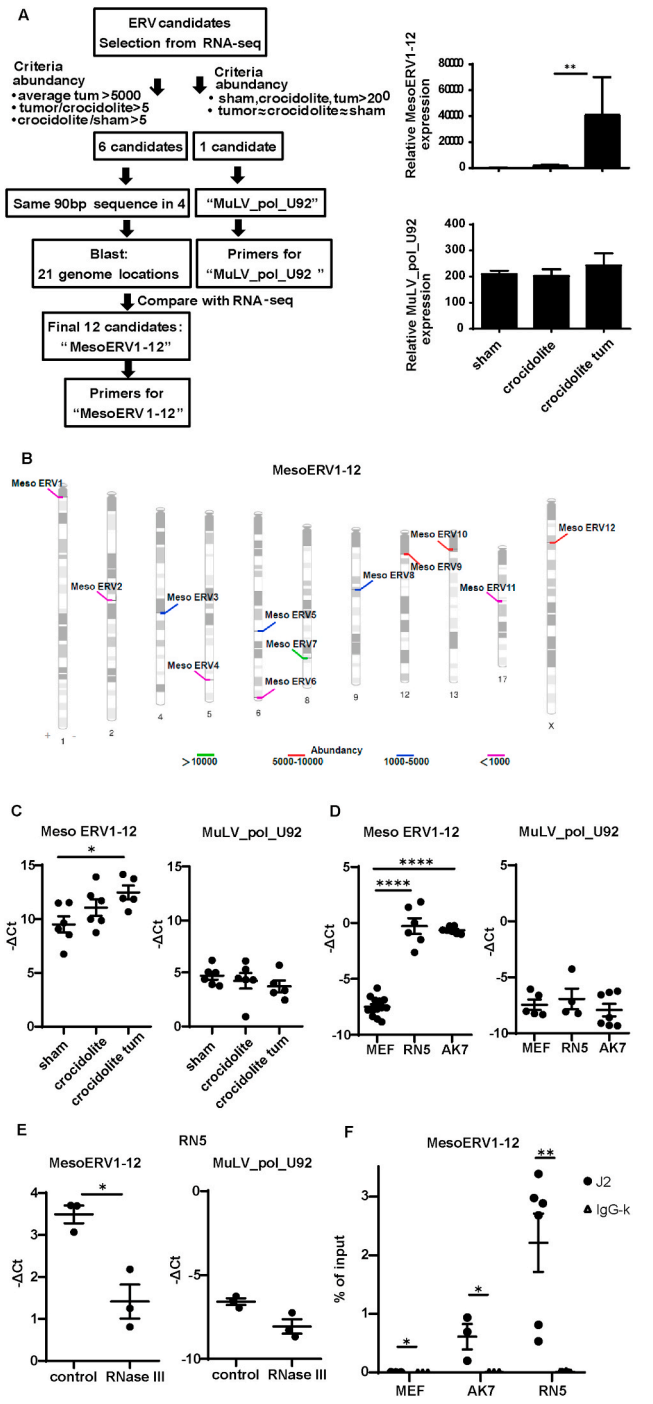

Fig. 2. "MesoERV1-12" are selectively expressed in mesothelioma and form dsRNA structure. (A) Steps to select the "MesoERV1-12"and "MuLV_pol_U92" (left panel) and their counts in RNA-seq data (right panel) (**) $P < 0.01$, Mann-Whitney test. (B) "MesoERV1-12" location and abundancy. The ideogram was created by Phenogram (http://visualization.ritchielab.org/phenograms/plot) [67]. Abundancy and strands annotation were added manually. (C) RT-qPCR validation of "MesoERV1-12" and "MuLV_pol_U92" expression in samples from mice exposed or not to crocidolite. (*) $P < 0.05$, Mann-Whitney test. (D) Basal expression of "Meso ERV1-12" and "MuLV_pol_U92" in mouse mesothelioma cells and Mouse Embryonic Fibroblasts (MEF), (****) $P < 0.0001$, unpaired *t*-test. (E) "MesoERV1-12" and "MuLV_pol_U92" expression in the presence or absence of RNaseIII digestion (*) $P < 0.05$, paired *t*-test. (F) RT-qPCR analysis of "MesoERV1-12" transcripts captured by J2 antibody in pulldown assay, (*) $P < 0.05$, (**) $P < 0.01$, paired t-tests.

In order to investigate whether "MesoERV1-12" and "MuLV_pol_U92" form dsRNA, total RNA was digested with RNaseIII (dsRNA cleavage enzyme) before cDNA synthesis and q-PCR. Treatment with RNaseIII significantly decreased "MesoERV1-12" detection (Fig. 2E) supporting the hypothesis that "MesoERV1-12" form dsRNA structures. This was also confirmed by RNA pull-down experiments using J2 anti-dsRNA antibody [30] which allowed enrichment of "MesoERV1-12" transcripts (Fig. 2F) in AK7 and RN5 mesothelioma cells.

3.2. Inhibition of DNMT leads to increased ERV and dsRNA expression in MEF cells

Next we aimed at investigating whether promoter demethylation was a possible cause for increased "MesoERV1-12" expression in mesothelioma, especially because, as previously mentioned, increased ERV expression has been observed after treatment with DNMT inhibitors [27]. In order to set up the experimental condition for the analysis of ERV promoter methylation, we designed an experiment based on our knowledge that "MesoERV1-12" is differentially expressed in MEF vs RN5 cells. DNA demethylation was induced in MEF by treatment with 5-Aza-2′-deoxycytidine (5-Aza-CdR), which is a DNMT inhibitor. Consistent with our hypothesis, this treatment significantly increased ERV expression in MEF, while "MuLV_pol_U92" remained at the same level (Fig. 3A and B). This was accompanied by a significant increase in dsRNA determined by using J2 [30] anti-dsRNA staining by flow cytometry (Fig. 3C) and RNaseIII digestion (Additional file2: Fig. S3).

Interestingly, although "MesoERV1-12" levels are high in RN5 and AK7 cells, their expression could be further increased by treatment with 5-Aza-CdR (Fig. 3D and E) and was accompanied by increased dsRNA levels (Fig. 3F).

3.3. Type I interferon signaling is activated in mesothelioma cells

dsRNA is part of the molecular patterns activating type-I IFN response, therefore we revisited the RNA-seq data from our previous study in crocidolite-exposed mice to investigate ISGs [31]. We applied the same criteria as in our previous analysis [9] ($p < 0.01$, FDR <0.012 and fold-change threshold higher than two-fold.). We observed, in addition to *Adar1,* an ISG that we have already described as significantly increased [9], 26 ISGs with an expression higher in tumor samples when compared to the samples from crocidolite-exposed mice with no tumor (Additional file1: Table S5). We then investigated the association of the expression of these genes with clinical outcome in mesothelioma patients of the TCGA [6] study and found that overexpression of 6 ISGs is associated with best overall survival (Additional file2: Fig. S4), consistent with patients who had a type-I IFN profile and showed a better clinical outcome [8].

We validated the increase of 2 of these genes, *DEAD (Asp-GluAla-Asp) box polypeptide 58* (*Ddx58*) and *interferon induced transmembrane protein 1 (Ifitm1)* in samples from asbestos-exposed mice (Fig. 4A). Activation of IFN signaling is further supported by Stat1 nuclear immunoreactivity present in these tissues (Additional file2: Fig. S5).

Next, we analyzed the expression of *Ddx58* and *Ifitm1* in MEF upon treatment with 5-Aza-CdR. We observed increased levels of *Ddx58* and *Ifitm1*, and confirmed that Rig-I (encoded by *Ddx58)* and Iftm1 proteins were also upregulated (Fig. 4B). As expected the expression of *type-I interferon beta* (*IFNB1*) was also increased (Fig. 4C). Similar changes were observed after MEF treatment with IFNβ1 (Additional file2: Fig. S6) confirming a functional type-I IFN signaling pathway. 5-Aza-CdR treatment-mediated stimulation of type-I signaling was further supported by increased levels of Irf3 phosphorylation (Fig. 4D), which is necessary to increase the expression of *IFNB1*.

In order to assess whether differential "MesoERV1-12" expression between MEF and mesothelioma cells is associated with a differential type-I IFN signaling activation, we determined that Rig-I and Ifitm1 expression levels are higher in mesothelioma RN5 and AK7 cells when

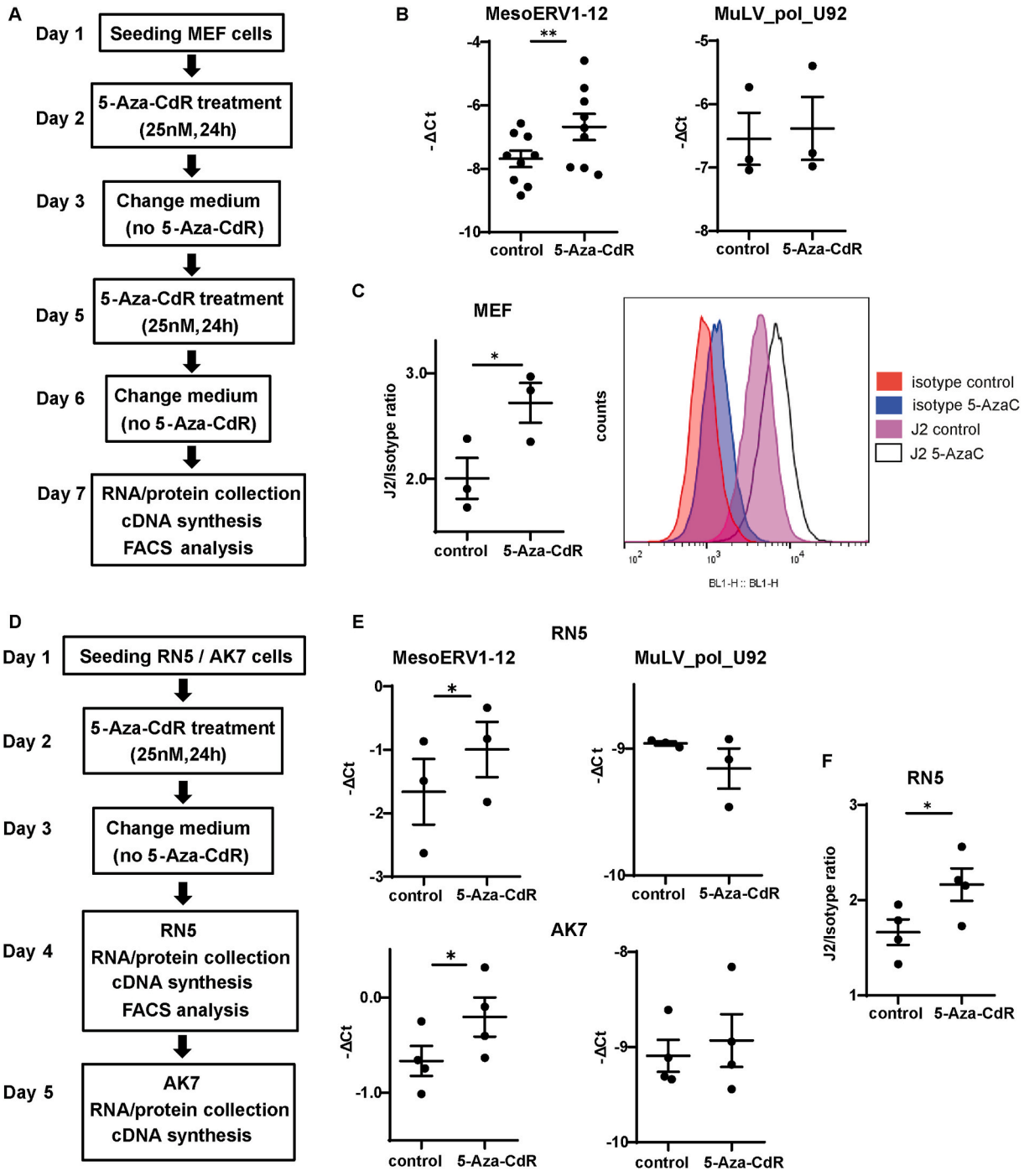

Fig. 3. dsRNA increases upon DNA-methyltransferase inhibitor treatment in MEF and mesothelioma cells. (A) Experimental protocol of 5-Aza-2′-deoxycytidine (5-Aza-CdR), a DNA methyltransferases inhibitor, treatment of MEF. (B) "MesoERV1-12" expression increased upon 5-Aza-CdR treatment in MEF (left panel), while "MuLV_pol_U92" expression did not change cells (right panel). (**) $P < 0.01$, paired *t*-test. (C) J2 anti-dsRNA immunoreactivity increased upon 5-Aza-CdR treatment in MEF (left panel). Representative shift of dsRNA-specific J2 stained population after 5-Aza-CdR treatment (right panel). (*) $P < 0.05$, paired *t*-test. (D) Experimental protocol of 5-Aza-CdR treatment on RN5 and AK7 mesothelioma cells. (E) "MesoERV1-12" expression increased with 5-Aza-CdR treatment in RN5 and AK7 mesothelioma cells, while "MuLV_pol_U92" expression did not change. (*) $P < 0.05$, paired *t*-test. (F) J2 anti-dsRNA staining increased upon 5-Aza-CdR treatment in RN5 cells. (*) $P < 0.05$, paired *t*-test.

compared to MEF (Fig. 4E). A basal activation of type-I IFN signaling was confirmed in RN5 cells by nuclear localization of Irf3 (Additional file2: Fig. S7).

To verify the involvement of dsRNA sensing we silenced mitochondrial antiviral signaling protein (Mavs), which is downstream of the activation of dsRNA sensors Rig-I and melanoma differentiation-associated protein 5. Silencing *Mavs* in RN5 mesothelioma cells resulted in a significant decrease of Rig-I and Ifitm1 (Fig. 4F).

Treatment of RN5 mesothelioma cells with Ruxolitinib, a JAK1/2 inhibitor blocking the type-I IFN signaling, or with an IFNAR1 (IFN-α/β receptor 1)-blocking antibody resulted in decreased levels of Rig-I and Ifitm1 (Fig. 5A and B).

Treatment of MEF with Ruxolitinib, decreased both basal and 5-Aza-CdR-induced levels of *Ddx58*, and *Ifitm1* (Fig. 5C).

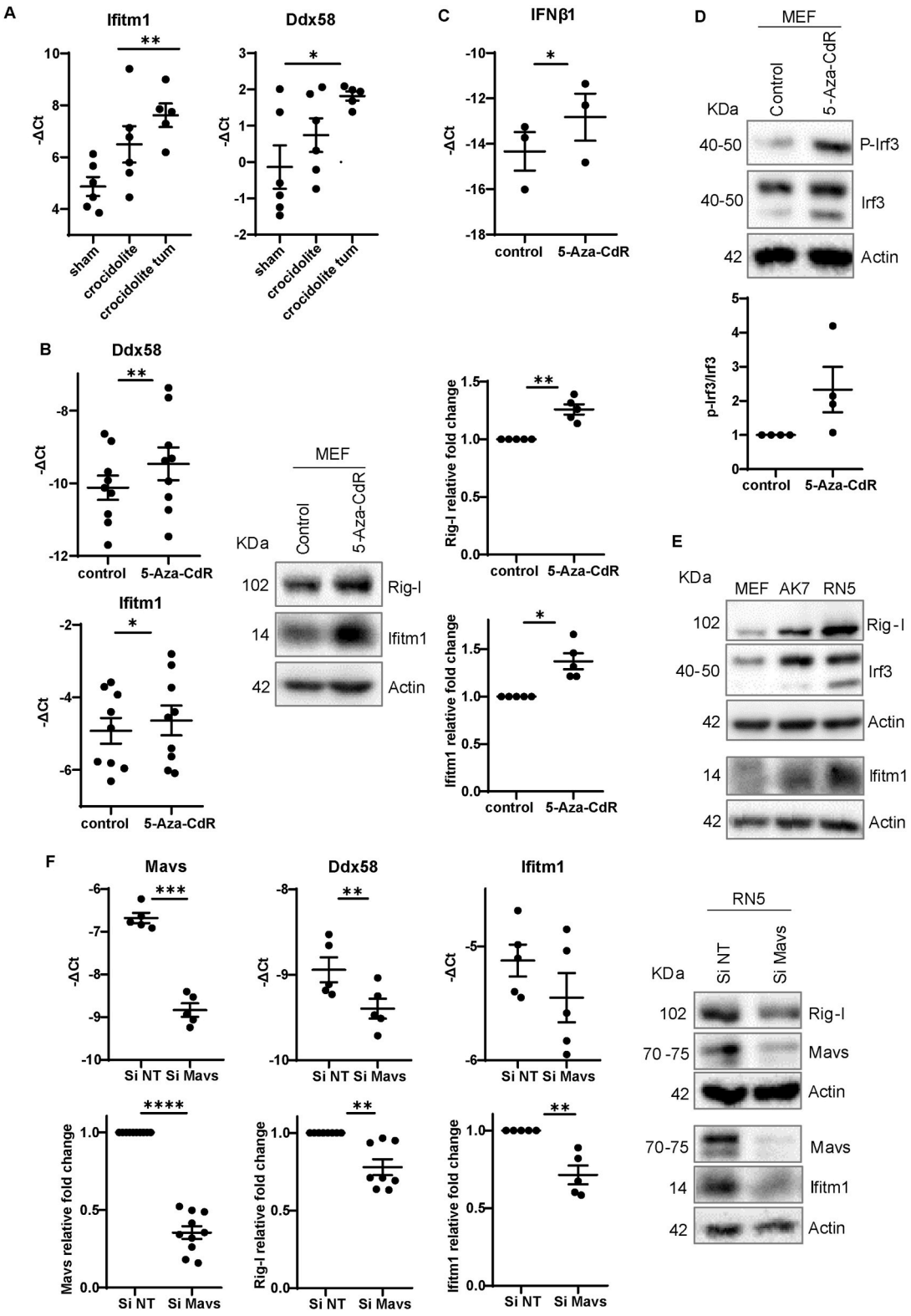

Fig. 4. Type-I IFN signaling increases upon DNA-methyltransferase inhibitor treatment in MEF and is high in RN5 and AK7 mouse mesothelioma cells. (A) The expression of interferon stimulated genes (ISG) *DEAD (Asp-Glu-Ala-Asp) box polypeptide 58 (Ddx58)* and *interferon induced transmembrane protein 1 (Ifitm1)* increased in the asbestos-exposed samples (*) $P < 0.05$, (**) $P < 0.01$, unpaired *t*-test. (B) The expression of Rig-I and Ifitm1 increased upon 5-Aza-CdR treatment in MEF. (*) $P < 0.05$, (**) $P < 0.01$, paired *t*-test. (C) The expression of type-I interferon beta *(Ifnβ1)* was increased upon 5-Aza-CdR treatment in MEF. (*) $P < 0.05$, paired *t*-test. (D) Phospho-Irf3 levels increased upon 5-Aza-CdR treatment in MEF. (E) The basal expression level of ISGs proteins in RN5 and AK7 cell lines is higher compared to MEF. (F) Silencing mitochondrial antiviral signaling (Mavs) decreased *Ddx58*, *Ifitm1* levels and their encoded proteins in RN5 mesothelioma cells. (**) $P < 0.01$, (***) $P < 0.001$, (****) $P < 0.0001$, paired *t*-test.

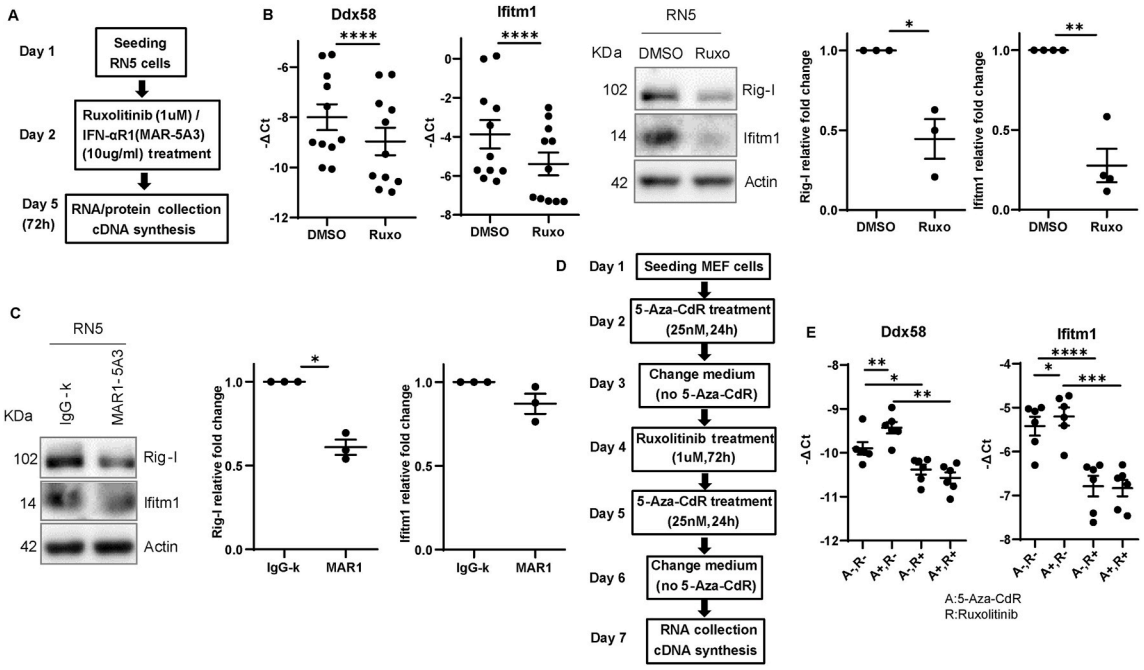

Fig. 5. Blocking the type-I IFN signaling decreased Rig-I and Ifitm1 in RN5 mesothelioma cells and Aza-CdR stimulated MEF . (A) Experimental protocol of Ruxolitinib (Ruxo), a JAK1/2 inhibitor or MAR1-5A3 (IFN-α/β receptor 1-blocking antibody) treatment in RN5 cells. (B) The expression of *Ddx58* and *Ifitm1* and their encoded proteins decreased after Ruxo treatment in RN5 cells. (*) $P < 0.05$, (**) $P < 0.01$, (****) $P < 0.0001$, paired *t*-test. (C) The expression of Rig-I and Ifitm1 decreased after MAR1-5A3 treatment in RN5 cells. (*) $P < 0.05$, paired *t*-test. (D) Experimental protocol of combination treatment of MEF cells with 5-Aza-CdR and Ruxo. (E) *Ddx58* and *Ifitm1* expression increased after 5-Aza-CdR treatment and decreased after adding Ruxo. (*) $P < 0.05$, (**) $P < 0.01$, (***) $P < 0.001$, (****) $P < 0.0001$, one-way ANOVA (Tukey's multiple comparisons test).

Altogether this data indicates that increased ISGs expression is dependent on type-I IFN receptor signaling.

3.4. Promoter methylation status decreases after 5-Aza-CdR treatment in RN5/MEF cells and in crocidolite exposed mice

In order to confirm that the increase in "*MesoERV1-12*" expression observed upon treatment with 5-Aza-CdR is due to promoter

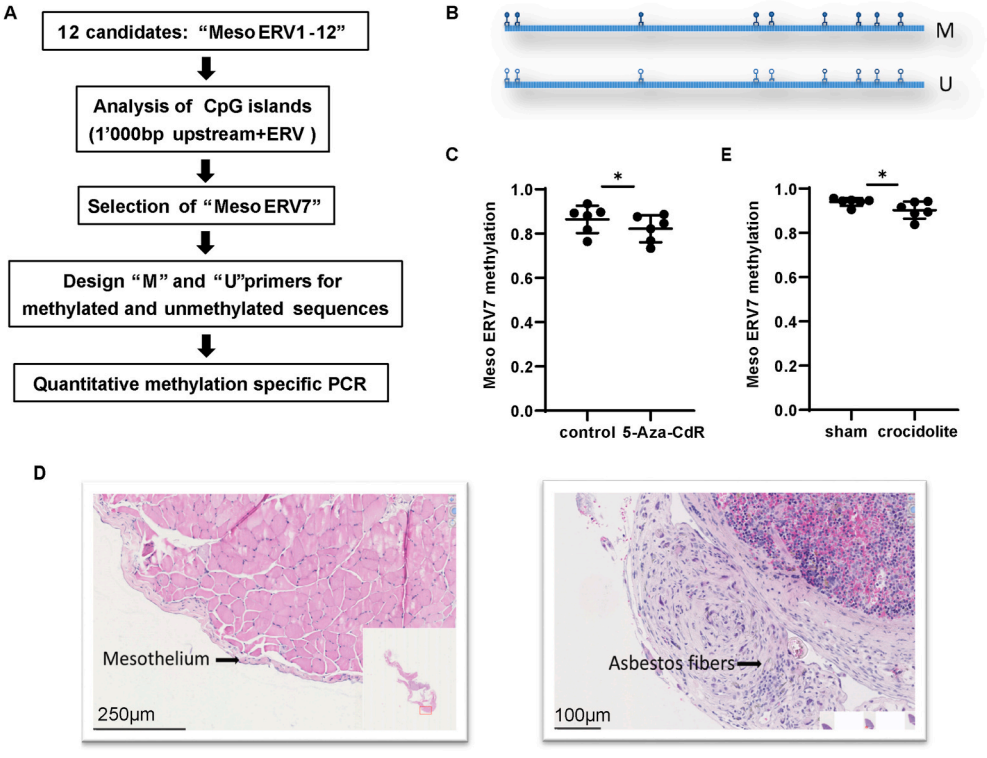

Fig. 6. Demethylation of MesoERV promoter upon mesothelioma development. (A) Steps to design the primers "M" and "U" to analyze the methylation status of "MesoERV7" promoter. "M": the pair of primers for CpGs methylated promoter sequence. "U": the pair of primers for CpGs unmethylated promoter sequence. (B) CpGs in the selected "MesoERV7" promoter fragment of 160 bp used for methylation analysis. (C) The fraction of "MesoERV7" promoter methylation decreased after 5-Aza-CdR treatment of RN5 cells. (*) $P < 0.05$, paired *t*-test. (D) Paraffin-embedded (FFPE) tissues of sham (left panel) or crocidolite (right panel) exposed mice. Mesothelium layer and asbestos fibers are indicated with an arrow. (E) The crocidolite exposed mice samples have more unmethylated CpGs in "MesoERV7" promoter. (*) $P < 0.05$, Mann Whitney test.

demethylation, we first identified (Fig. 6A) "MesoERV7" as the best target region based on the analysis of CpG islands (Additional file2: Fig. S8a). With the help of an online platform MethPrimer [19] we designed methylation-specific primer "M" and unmethylation-specific primer "U" for a 160 bp region of the promoter of "MesoERV7", which has 9 CpG sites (Fig. 6B), shown to be methylated using whole genome bisulfite sequencing (Additional file2: Fig. S8b) [32]. These primers were used on sodium bisulfite treated DNA, where all methyl-free cytosines are converted into uracils, whereas methylated cytosines remain unchanged allowing the use of quantitative methylation specific PCR (qMSP).

In RN5 cells, "MesoERV7" promoter methylation decreased significantly upon 5-Aza-CdR treatment (Fig. 6C). Low levels of basal demethylation rendered impossible to perform qMSP measurement in MEF, because the U primers were producing two additional major fragments. However, the demethylated "MesoERV7" promoter fragment was increased after 5-Aza-CdR treatment (Additional file2: Fig. S9), confirming that epigenetic silencing controls "MesoERV7" expression.

gDNA was extracted from formalin-fixed, paraffin-embedded (FFPE) tissues from sham or crocidolite exposed mice (Fig. 6D). We performed the same bisulfite treatment as above followed by qMSP and observed that "MesoERV7" promoter is significantly more demethylated in tissues from crocidolite exposed mice compared to sham mice (Fig. 6E). Low effect size is possibly due to contaminating non-tumor cells.

Altogether our data suggest that during mesothelioma development demethylation events trigger ERV expression, thereby increasing dsRNA levels able to activate type-I IFN.

4. Discussion

In this study we report that mesothelioma development is associated with increased expression of ERV forming dsRNA, thereby leading to type-I IFN activation in the absence of viral pathogens.

Our observations are consistent with mesothelioma being a cancer highly enriched for the 38-ISG signature not always justified by the presence of immune cells in the microenvironment [4]. Eight ISGs of the signature (ADAR1, OASL, ISG15, RSAD2, ISG20, IFIT2, MX1 and IFIT3) overlap with genes found to be significantly overexpressed in mesothelioma samples compared to mesothelial tissue obtained after mice exposure to crocidolite [9]. In the present study we used as readout genes (*Ddx58 and Ifitm1*) that are overexpressed in crocidolite-induced mesothelioma experimental samples, and which are associated with the clinical outcome in mesothelioma patients.

It had already been observed that primary mesothelioma cells maintain the activation of the type-I IFN signaling pathway [5] but the underlying mechanisms were not known. We observed a progressive increase of Adar-dependent dsRNA editing of non-coding regions from sham to crocidolite-exposed tissue to crocidolite exposed tumors, and we demonstrate that dsRNA activates type-I IFN response, which is in line with the known role of Adar1 as a negative regulator of type-I IFN signaling [33,34]. Of all non-coding dsRNA forming potential targets, we focused on the analysis of ERV for several reasons. First, ERV have already been described to be edited by ADAR [10,24–26] implicating that they form dsRNA structures, and this is also suggested using RNA folding predictive tools on e.g. "MesoERV7" (Additional file2: Fig. S10). Second, we observed increased expression of these ERV sequences upon mesothelioma development; therefore, investigation of the mechanisms leading to their expression may shed light on tumorigenesis. Third, induction of the expression of ERV has been documented in studies supporting the use of viral mimicry in clinical trials where effects of immune checkpoint inhibitor are tested in combination with demethylating agents [27,35]. ERV expression is a predictor of patient response to immunotherapy in an urothelial cancer cohort [36] and, interestingly, in that study it was a better predictor compared to type-I IFN signature. In addition, high ERV expression was associated with better overall clinical outcome in a cohort of melanoma patients while repression of ERV was observed in the cohort with worst outcome [37].

Increased expression of dsRNA and ISGs upon treatment with cytotoxic concentration of demethylating agents had already been observed in p53-deficient but not p53 wt-MEF [38], while in our study these events could be detected in p53 wt-MEF. Possible reasons for this difference are the use of lower concentrations of 5-Aza-CdR in our study. The advantage of using p53 wt-MEF is to avoid confounding factors, since p53 deficient-MEF have a basal activation of the innate immune system compared to p53 wt-MEF due to increased levels of cytosolic dsRNA deriving from mitochondrial DNA [39].

Changes in DNA methylation have already been documented in human mesothelioma [40] and silencing of tumor suppressor genes was associated with asbestos exposure [41]. In a later more comprehensive study, almost 3-times more CpG sites were found that were less methylated in mesothelioma as compared to the normal pleura [42], demonstrating large demethylation events in mesothelioma, but they were not further investigated.

Epigenetic events occur at early stages during mesothelioma development as documented by increased levels of DNA methylation at the *ink4a* locus after mice exposure to asbestos [43]. The *ink4a* locus encodes for a tumor suppressor frequently inactivated in mesothelioma (reviewed in Ref. [1]). In the current study, we describe hypomethylation of a selected ERV promoter associated with increased ERV expression and generation of dsRNA. Consequently, stimulation of type-I IFN pathway is observed. Interestingly in the TCGA study [6] both type-I IFN signaling and methylation status are associated with the status of BRCA1-associated protein (BAP1), a tumor suppressor gene, which is also frequently inactivated in mesothelioma (reviewed in Ref. [1]) however the underlying mechanisms are not clear. Nevertheless, we recently described that Measle Virus (MV)-resistant cell lines showed a significantly lower BAP1 expression than MV-sensitive cell lines [44] and a recent analysis of TCGA public available data revealed a negative correlation between BAP1 expression and a constitutively activated type-I IFN response [45].

ERV sequences are part of embryonically active elements, which are often hypomethylated, thereby de-repressed, in cancer, and a recent analysis of TCGA data has revealed upregulation of ERV sequences in several cancer types [46]. Indeed, DNA methylation at CpG along with histone methylation constitutes the major mechanism of transcriptional control of ERVs (reviewed in Ref. [47]). We observed downregulation of *Dnmt3a* and upregulation of *Tet3*, *Dnmt, Dnmt3b* and *Dnmt3l* in tumors tissue (Additional file2: Fig. S11). Dnmt3l associates with Dnmt3a and Dnmt3b to stimulate their enzymatic activities [48]. Our observation is consistent with the knowledge that DNMT1 and DNMT3B but not DNMT3A have an essential role in cancer cells [49,50] and the observation that silencing of DNMT1 and DNMT3B resulted in inhibition of mesothelioma cell growth [51]. In addition, more recently E3 ubiquitin ligases UHRF1/2 have been shown to negatively regulate DNMT3A as mechanism for widespread DNA hypomethylation in cancer resulting in ERV upregulation [52]. UHRF1 is upregulated in mesothelioma and it is upregulated in normal mesothelial cells after exposure to crocidolite [53]. Both *Uhrf1* and *Uhrf2* are upregulated in mouse tumor tissue (Additional file2: Fig. S11), suggesting a possible implication of these enzymes in ERV upregulation.

In mammals, CpG methylation is initiated by the de novo methyltransferases including DNMT3A, 3B and is perpetuated across mitosis by the maintenance DNA methyltransferase DNMT1. DNA demethylation occurs passively during DNA replication or actively via demethylation by ten-eleven translocations (TET) enzymes, which catalyze oxidation of 5-methylcytosine to 5- hydroxymethylcytosine, 5-formylcytosine, and 5-carboxylcytosine [54]. In an experimental model of mesothelioma development after rats exposure to asbestos, a significant decreased in expression of DNMT3A and 3B has been observed accompanied by increased levels of 5- hydroxymethylcytosine [55], which is consistent with our observation that epigenetic events increase ERV expression. Altogether these observations suggest that it might be worth

investigating circulating cell-free DNA (cfDNA) methylation and hydroxymethylation in plasma for early mesothelioma detection as shown for other cancers [56,57].

Other examples of genes demethylated in mesothelioma as compared to normal tissue are tumor-associated antigens [58] and their expression can be increased after treatment with hypomethylating drugs including in mesothelioma patients [17,58–60]. One of these studies was performed by *in vivo* testing of epigenetic drugs in an experimental syngeneic model using AK7 mouse mesothelioma cells, and we show in our study that these cells also express "MesoERV1-12". In the *in vivo* study, treatment with 5-Aza-CdR showed an effect on lymphocyte aggregation and it is possible that increased expression of type-I IFN signaling was a contributing factor along with increased expression of tumor-associated antigens.

This is the first study demonstrating that increased ADAR-dependent editing observed during mesothelioma development is associated with demethylation-induced expression of ERV able to form dsRNA, thereby activating type-I IFN signaling. In the broader context of mesothelioma, our observations that "MesoERV1-12" expression increases upon mesothelioma development opens a novel perspective not explored in the current study. Indeed, it is known that high level of transcription of several ERV loci promotes the expression of long noncoding RNAs [61], which appear important in controlling cell identity [62,63]. Future studies should address this issue. In addition, it is likely that ERV promoter demethylation and expression is part of a much larger demethylation-induced production of dsRNA forming non-coding sequences such as SINE and satellite DNA [38], which remains to be explored, also in the context of early diagnosis.

Our observation is also important for mesothelioma therapy. Indeed, therapeutic approaches exploiting type-I IFN pathway signaling have already been implemented in the clinic [64] or proposed on the basis of preclinical studies [65,66]. Future studies will investigate whether ERV expression could be a predictor of sensitivity to those therapeutic approaches, although it should be taken into account that for those therapies inducing type-I IFN signaling, some mesothelioma have lost the type-I IFN genes [2] and might therefore not be able to activate such signaling.

Research data for this article

The datasets supporting the conclusions of this article are available in the Zenodo repository, (10.5281/zenodo.4088000). RNA-seq data are deposited in the European Nucleotide Archive, accession no PRJEB15230. Endogenous Viral Elements (EVE) database is available on http://geve.med.u-tokai.ac.jp/download/. Software: Software and resources used for the analyses are described in the paper.

CRediT authorship contribution statement

Suna Sun: Investigation, Methodology, Data curation, Formal analysis, Validation, Writing – original draft, Writing – review & editing. **Francesca Frontini:** Investigation, Methodology. **Weihong Qi:** Data curation, Formal analysis. **Ananya Hariharan:** Investigation, Methodology, Writing – review & editing. **Manuel Ronner:** Investigation, Methodology, Validation. **Martin Wipplinger:** Investigation, Methodology. **Christophe Blanquart:** Resources. **Hubert Rehrauer:** Conceptualization, Data curation, Formal analysis. **Jean-François Fonteneau:** Conceptualization, Resources, Writing – review & editing. **Emanuela Felley-Bosco:** Conceptualization, Supervision, Funding acquisition, Project administration, Writing – original draft, Writing – review & editing.

Declaration of competing interest

The authors declare that they have no competing interests.

Acknowledgements

This work was supported by Swiss National Science Foundation grant 320030_182690, Walter-Bruckerhoff Stiftung and Stiftung für Angewandte Krebsforchung, "La Ligue Régionale Grand Ouest contre le Cancer" (CSIRGO: CD16, CD22, CD41, CD44, CD49, CD56, CD72, CD79 and CD85) et "La Fondation ARC". Suna Sun is supported by China Scholarship Council (CSC). FF was supported by IUSS Ferrara PhD students mobility 2019, Associazione Italiana Biologia e Genetica Generale e Molecolare contribution for research abroad 2019 and Consorzio Interuniversitario Biotecnologie award for stays and training activities at foreign institutions.

Appendix A. Supplementary data

Supplementary data to this article can be found online at https://doi.org/10.1016/j.canlet.2021.03.004.

References

[1] M. Carbone, P.S. Adusumilli, H.R. Alexander Jr., P. Baas, F. Bardelli, A. Bononi, R. Bueno, E. Felley-Bosco, F. Galateau-Salle, D. Jablons, A.S. Mansfield, M. Minaai, M. de Perrot, P. Pesavento, V. Rusch, D.T. Severson, E. Taioli, A. Tsao, G. Woodard, H. Yang, M.G. Zauderer, H.I. Pass, Mesothelioma: Scientific clues for prevention, diagnosis, and therapy, CA A Cancer J. Clin. 69 (2019) 402–429.

[2] T. Delaunay, C. Achard, N. Boisgerault, M. Grard, T. Petithomme, C. Chatelain, S. Dutoit, C. Blanquart, P.J. Royer, S. Minvielle, L. Quetel, C. Meiller, D. Jean, D. Fradin, J. Bennouna, A. Magnan, L. Cellerin, F. Tangy, M. Gregoire, J. F. Fonteneau, Frequent homozygous deletions of Type I interferon genes in pleural mesothelioma confer sensitivity to oncolytic measles virus, J. Thorac. Oncol. 15 (2020) 827–842.

[3] S.G. Gray, L. Mutti, Immunotherapy for mesothelioma: a critical review of current clinical trials and future perspectives, Transl. Lung Cancer Res. 9 (2020) S100–S119.

[4] H. Liu, J. Golji, L.K. Brodeur, F.S. Chung, J.T. Chen, R.S. deBeaumont, C.P. Bullock, M.D. Jones, G. Kerr, L. Li, D.P. Rakiec, M.R. Schlabach, S. Sovath, J.D. Growney, R. A. Pagliarini, D.A. Ruddy, K.D. MacIsaac, J.M. Korn, E.R. McDonald 3rd, Tumor-derived IFN triggers chronic pathway agonism and sensitivity to ADAR loss, Nat. Med. 25 (2019) 95–102.

[5] T. Chernova, X.M. Sun, I.R. Powley, S. Galavotti, S. Grosso, F.A. Murphy, G. J. Miles, L. Cresswell, A.V. Antonov, J. Bennett, A. Nakas, D. Dinsdale, K. Cain, M. Bushell, A.E. Willis, M. MacFarlane, Molecular profiling reveals primary mesothelioma cell lines recapitulate human disease, Cell Death Differ. 23 (2016) 1152–1164.

[6] J. Hmeljak, F. Sanchez-Vega, K.A. Hoadley, J. Shih, C. Stewart, D.I. Heiman, P. Tarpey, L. Danilova, E. Drill, E.A. Gibb, R. Bowlby, R. Kanchi, H. U. Osmanbeyoglu, Y. Sekido, J. Takeshita, Y. Newton, K. Graim, M. Gupta, C. M. Gay, L. Diao, D.L. Gibbs, V. Thorsson, L. Iype, H.S. Kantheti, D.T. Severson, G. Ravegnini, P. Desmeules, A.A. Jungbluth, W.D. Travis, S. Dacic, L.R. Chirieac, F. Galateau-Salle, J. Fujimoto, A.N. Husain, H.C. Silveira, V.W. Rusch, R.C. Rintoul, H. Pass, H. Kindler, M.G. Zauderer, D.J. Kwiatkowski, R. Bueno, A.S. Tsao, J. Creaney, T. Lichtenberg, K. Leraas, J. Bowen, T. Research Network, I. Felau, J. C. Zenklusen, R. Akbani, A.D. Cherniack, L.A. Byers, M.S. Noble, J.A. Fletcher, G. Robertson, R. Shen, H. Aburatani, B.W. Robinson, P. Campbell, M. Ladanyi, Integrative molecular characterization of malignant pleural mesothelioma, Canc. Discov. 8 (2018) 1548–1565.

[7] R. Bueno, E.W. Stawiski, L.D. Goldstein, S. Durinck, A. De Rienzo, Z. Modrusan, F. Gnad, T.T. Nguyen, B.S. Jaiswal, L.R. Chirieac, D. Sciaranghella, N. Dao, C. E. Gustafson, K.J. Munir, J.A. Hackney, A. Chaudhuri, R. Gupta, J. Guillory, K. Toy, C. Ha, Y.J. Chen, J. Stinson, S. Chaudhuri, N. Zhang, T.D. Wu, D.J. Sugarbaker, F. J. de Sauvage, W.G. Richards, S. Seshagiri, Comprehensive genomic analysis of malignant pleural mesothelioma identifies recurrent mutations, gene fusions and splicing alterations, Nat. Genet. 48 (2016) 407–416.

[8] TCGA. http://gdac.broadinstitute.org/runs/analyses_2014_10_17/reports/cancer/MESO-TP/Correlate_Clinical_vs_Molecular_Subtypes/nozzle.html, 2014.

[9] H. Rehrauer, L. Wu, W. Blum, L. Pecze, T. Henzi, V. Serre-Beinier, C. Aquino, B. Vrugt, M. de Perrot, B. Schwaller, E. Felley-Bosco, How asbestos drives the tissue towards tumors: YAP activation, macrophage and mesothelial precursor recruitment, RNA editing, and somatic mutations, Oncogene 37 (2018) 2645–2659.

[10] K. Nishikura, A-to-I editing of coding and non-coding RNAs by ADARs, Nat. Rev. Mol. Cell Biol. 17 (2016) 83–96.

[11] S.W. Brubaker, K.S. Bonham, I. Zanoni, J.C. Kagan, Innate immune pattern recognition: a cell biological perspective, Annu. Rev. Immunol. 33 (2015) 257–290.

[12] A. Hariharan, S. Suna, M. Wipplinger, E. Felley-Bosco, RNA editing in mesothelioma: a look forward, Open Biol. 10 (2020).

[13] R. Lower, J. Lower, R. Kurth, The viruses in all of us: characteristics and biological significance of human endogenous retrovirus sequences, Proc. Natl. Acad. Sci. U. S. A. 93 (1996) 5177–5184.

[14] W. Blum, L. Pecze, E. Felley-Bosco, J. Worthmuller-Rodriguez, L. Wu, B. Vrugt, M. de Perrot, B. Schwaller, Establishment of immortalized murine mesothelial cells and a novel mesothelioma cell line, in Vitro Cell, Dev. Biol. Anim. 51 (2015) 714–721.
[15] P.A. Moalli, J.L. MacDonald, L.A. Goodglick, A.B. Kane, Acute injury and regeneration of the mesothelium in response to asbestos fibers, Am. J. Pathol. 128 (1987) 426–445.
[16] M.R. Davis, L.S. Manning, D. Whitaker, M.J. Garlepp, B.W. Robinson, Establishment of a murine model of malignant mesothelioma, Int. J. Canc. 52 (1992) 881–886.
[17] J. Kresoja-Rakic, E. Kapaklikaya, G. Ziltener, D. Dalcher, R. Santoro, B. C. Christensen, K.C. Johnson, B. Schwaller, W. Weder, R.A. Stahel, E. Felley-Bosco, Identification of cis- and trans-acting elements regulating calretinin expression in mesothelioma cells, Oncotarget 7 (2016) 21272–21286.
[18] J. Kresoja-Rakic, E. Felley-Bosco, Desthiobiotin-streptavidin-affinity mediated purification of rna-interacting proteins in mesothelioma cells, J Vis Exp 134 (2018), 57516, https://doi.org/10.3791/57516.
[19] L.C. Li, R. Dahiya, MethPrimer: designing primers for methylation PCRs, Bioinformatics 18 (2002) 1427–1431.
[20] C. Furlan, J. Polesel, L. Barzan, G. Franchin, S. Sulfaro, S. Romeo, F. Colizzi, A. Rizzo, V. Baggio, V. Giacomarra, A.P. Dei Tos, P. Boscolo-Rizzo, E. Vaccher, R. Dolcetti, L. Sigalotti, E. Fratta, Prognostic significance of LINE-1 hypomethylation in oropharyngeal squamous cell carcinoma, Clin. Epigenet. 9 (2017) 58.
[21] Y. Jin, O.H. Tam, E. Paniagua, M. Hammell, TEtranscripts: a package for including transposable elements in differential expression analysis of RNA-seq datasets, Bioinformatics 31 (2015) 3593–3599.
[22] S.H. Roth, E.Y. Levanon, E. Eisenberg, Genome-wide quantification of ADAR adenosine-to-inosine RNA editing activity, Nat. Methods 16 (2019) 1131–1138.
[23] K.A. Lehmann, B.L. Bass, Double-stranded RNA adenosine deaminases ADAR1 and ADAR2 have overlapping specificities, Biochemistry 39 (2000) 12875–12884.
[24] K. Licht, U. Kapoor, F. Amman, E. Picardi, D. Martin, P. Bajad, M.F. Jantsch, A high resolution A-to-I editing map in the mouse identifies editing events controlled by pre-mRNA splicing, Genome Res. 29 (2019) 1453–1463.
[25] M.G. Blango, B.L. Bass, Identification of the long, edited dsRNAome of LPS-stimulated immune cells, Genome Res. 26 (2016) 852–862.
[26] H. Chung, J.J.A. Calis, X. Wu, T. Sun, Y. Yu, S.L. Sarbanes, V.L. Dao Thi, A. R. Shilvock, H.H. Hoffmann, B.R. Rosenberg, C.M. Rice, Human ADAR1 prevents endogenous RNA from triggering translational shutdown, Cell 172 (2018) 811–824, e814.
[27] K.B. Chiappinelli, P.L. Strissel, A. Desrichard, H. Li, C. Henke, B. Akman, A. Hein, N.S. Rote, L.M. Cope, A. Snyder, V. Makarov, S. Budhu, D.J. Slamon, J.D. Wolchok, D.M. Pardoll, M.W. Beckmann, C.A. Zahnow, T. Merghoub, T.A. Chan, S.B. Baylin, R. Strick, Inhibiting DNA methylation causes an interferon response in cancer via dsRNA including endogenous retroviruses, Cell 162 (2015) 974–986.
[28] E.B. Chuong, N.C. Elde, C. Feschotte, Regulatory evolution of innate immunity through co-option of endogenous retroviruses, Science 351 (2016) 1083–1087.
[29] L. Gagnier, V.P. Belancio, D.L. Mager, Mouse germ line mutations due to retrotransposon insertions, Mobile DNA 10 (2019) 15.
[30] F. Weber, V. Wagner, S.B. Rasmussen, R. Hartmann, S.R. Paludan, Double-stranded RNA is produced by positive-strand RNA viruses and DNA viruses but not in detectable amounts by negative-strand RNA viruses, J. Virol. 80 (2006) 5059–5064.
[31] W.M. Schneider, M.D. Chevillotte, C.M. Rice, Interferon-stimulated genes: a complex web of host defenses, Annu. Rev. Immunol. 32 (2014) 513–545.
[32] C.G. Duncan, H.D. Kondilis-Mangum, S.A. Grimm, P.R. Bushel, K. Chrysovergis, J. D. Roberts, F.L. Tyson, B.A. Merrick, P.A. Wade, Base-resolution analysis of DNA methylation patterns downstream of Dnmt3a in Mouse Naive B cells, G3 (Bethesda) 8 (2018) 805–813.
[33] C.E. Samuel, Adenosine deaminase acting on RNA (ADAR1), a suppressor of double-stranded RNA-triggered innate immune responses, J. Biol. Chem. 294 (2019) 1710–1720.
[34] N.M. Mannion, S.M. Greenwood, R. Young, S. Cox, J. Brindle, D. Read, C. Nellaker, C. Vesely, C.P. Ponting, P.J. McLaughlin, M.F. Jantsch, J. Dorin, I.R. Adams, A. D. Scadden, M. Ohman, L.P. Keegan, M.A. O'Connell, The RNA-editing enzyme ADAR1 controls innate immune responses to RNA, Cell Rep. 9 (2014) 1482–1494.
[35] D. Roulois, H. Loo Yau, R. Singhania, Y. Wang, A. Danesh, S.Y. Shen, H. Han, G. Liang, P.A. Jones, T.J. Pugh, C. O'Brien, D.D. De Carvalho, DNA-demethylating agents target colorectal cancer cells by inducing viral mimicry by endogenous transcripts, Cell 162 (2015) 961–973.
[36] A. Solovyov, N. Vabret, K.S. Arora, A. Snyder, S.A. Funt, D.F. Bajorin, J. E. Rosenberg, N. Bhardwaj, D.T. Ting, B.D. Greenbaum, Global cancer transcriptome quantifies repeat element polarization between immunotherapy responsive and t cell suppressive classes, Cell Rep. 23 (2018) 512–521.
[37] B. Badal, A. Solovyov, S. Di Cecilia, J.M. Chan, L.W. Chang, R. Iqbal, I.T. Aydin, G. S. Rajan, C. Chen, F. Abbate, K.S. Arora, A. Tanne, S.B. Gruber, T.M. Johnson, D. R. Fullen, L. Raskin, R. Phelps, N. Bhardwaj, E. Bernstein, D.T. Ting, G. Brunner, E. E. Schadt, B.D. Greenbaum, J.T. Celebi, Transcriptional dissection of melanoma identifies a high-risk subtype underlying TP53 family genes and epigenome deregulation, JCI Insight (2017) 2.
[38] K.I. Leonova, L. Brodsky, B. Lipchick, M. Pal, L. Novototskaya, A.A. Chenchik, G. C. Sen, E.A. Komarova, A.V. Gudkov, p53 cooperates with DNA methylation and a suicidal interferon response to maintain epigenetic silencing of repeats and noncoding RNAs, Proc. Natl. Acad. Sci. U. S. A. 110 (2013) E89–E98.
[39] D.M. Wiatrek, M.E. Candela, J. Sedmik, J. Oppelt, L.P. Keegan, M.A. O'Connell, Activation of innate immunity by mitochondrial dsRNA in mouse cells lacking p53 protein, RNA 25 (2019) 713–726.
[40] A. Destro, G.L. Ceresoli, E. Baryshnikova, I. Garassino, P.A. Zucali, F. De Vincenzo, P. Bianchi, E. Morenghi, A. Testori, M. Alloisio, A. Santoro, M. Roncalli, Gene methylation in pleural mesothelioma: correlations with clinico-pathological features and patient's follow-up, Lung Canc. 59 (2007) 369–376.
[41] B.C. Christensen, J.J. Godleski, C.J. Marsit, E.A. Houseman, C.Y. Lopez-Fagundo, J. L. Longacker, R. Bueno, D.J. Sugarbaker, H.H. Nelson, K.T. Kelsey, Asbestos exposure predicts cell cycle control gene promoter methylation in pleural mesothelioma, Carcinogenesis 29 (2008) 1555–1559.
[42] B.C. Christensen, E.A. Houseman, J.J. Godleski, C.J. Marsit, J.L. Longacker, C. R. Roelofs, M.R. Karagas, M.R. Wrensch, R.F. Yeh, H.H. Nelson, J.L. Wiemels, S. Zheng, J.K. Wiencke, R. Bueno, D.J. Sugarbaker, K.T. Kelsey, Epigenetic profiles distinguish pleural mesothelioma from normal pleura and predict lung asbestos burden and clinical outcome, Canc. Res. 69 (2009) 227–234.
[43] T. Chernova, F.A. Murphy, S. Galavotti, X.M. Sun, I.R. Powley, S. Grosso, A. Schinwald, J. Zacarias-Cabeza, K.M. Dudek, D. Dinsdale, J. Le Quesne, J. Bennett, A. Nakas, P. Greaves, C.A. Poland, K. Donaldson, M. Bushell, A.E. Willis, M. MacFarlane, Long-fiber carbon nanotubes replicate asbestos-induced mesothelioma with disruption of the tumor suppressor gene Cdkn2a (Ink4a/Arf), Curr. Biol. 27 (2017) 3302–3314 e3306.
[44] D. Jean, T. Delaunay, C. Meiller, N. Boisgerault, M. Grard, S. Caruso, C. Blanquart, E. Felley-Bosco, J. Bennouna, F. Tangy, M. Gregoire, J.F. Fonteneau, Reply to: oncolytic viral therapy for malignant pleural mesothelioma, J. Thorac. Oncol. 15 (2020) e113–e116.
[45] H. Yang, D. Xu, Y. Gao, R.A. Schmid, R.W. Peng, The association of BAP1 loss-of-function with the defect in homologous recombination repair and sensitivity to PARP-targeted therapy, J. Thorac. Oncol. 15 (2020) e88–e90.
[46] M.S. Rooney, S.A. Shukla, C.J. Wu, G. Getz, N. Hacohen, Molecular and genetic properties of tumors associated with local immune cytolytic activity, Cell 160 (2015) 48–61.
[47] M. Friedli, D. Trono, The developmental control of transposable elements and the evolution of higher species, Annu. Rev. Cell Dev. Biol. 31 (2015) 429–451.
[48] I. Suetake, F. Shinozaki, J. Miyagawa, H. Takeshima, S. Tajima, DNMT3L stimulates the DNA methylation activity of Dnmt3a and Dnmt3b through a direct interaction, J. Biol. Chem. 279 (2004) 27816–27823.
[49] N. Beaulieu, S. Morin, I.C. Chute, M.F. Robert, H. Nguyen, A.R. MacLeod, An essential role for DNA methyltransferase DNMT3B in cancer cell survival, J. Biol. Chem. 277 (2002) 28176–28181.
[50] M.F. Robert, S. Morin, N. Beaulieu, F. Gauthier, I.C. Chute, A. Barsalou, A. R. MacLeod, DNMT1 is required to maintain CpG methylation and aberrant gene silencing in human cancer cells, Nat. Genet. 33 (2003) 61–65.
[51] E.S. Kassis, M. Zhao, J.A. Hong, G.A. Chen, D.M. Nguyen, D.S. Schrump, Depletion of DNA methyltransferase 1 and/or DNA methyltransferase 3b mediates growth arrest and apoptosis in lung and esophageal cancer and malignant pleural mesothelioma cells, J. Thorac. Cardiovasc. Surg. 131 (2006) 298–306.
[52] Y. Jia, P. Li, L. Fang, H. Zhu, L. Xu, H. Cheng, J. Zhang, F. Li, Y. Feng, Y. Li, J. Li, R. Wang, J.X. Du, J. Li, T. Chen, H. Ji, J. Han, W. Yu, Q. Wu, J. Wong, Negative regulation of DNMT3A de novo DNA methylation by frequently overexpressed UHRF family proteins as a mechanism for widespread DNA hypomethylation in cancer, Cell Discov. 2 (2016) 16007.
[53] E.S. Reardon, V. Shukla, S. Xi, S.K. Gara, Y. Liu, D. Straughan, M. Zhang, J.A. Hong, E.C. Payabyab, A. Kumari, W.G. Richards, A. De Rienzo, R. Hassan, M. Miettinen, L. Xi, M. Raffeld, L.T. Uechi, X. Li, R. Wang, H. Chen, C.D. Hoang, R. Bueno, D. S. Schrump, UHRF1 is a novel druggable epigenetic target in malignant pleural mesothelioma, J. Thorac. Oncol. 16 (2021) 89–103.
[54] M. Bochtler, A. Kolano, G.L. Xu, DNA demethylation pathways: additional players and regulators, Bioessays 39 (2017) 1–13.
[55] D. Roulois, S. Deshayes, M.N. Guilly, J.S. Nader, C. Liddell, M. Robard, P. Hulin, A. Ouacher, V. Le Martelot, J.F. Fonteneau, M. Gregoire, C. Blanquart, D. L. Pouliquen, Characterization of preneoplastic and neoplastic rat mesothelial cell lines: the involvement of TETs, DNMTs, and 5-hydroxymethylcytosine, Oncotarget 7 (2016) 34664–34687.
[56] S.Y. Shen, R. Singhania, G. Fehringer, A. Chakravarthy, M.H.A. Roehrl, D. Chadwick, P.C. Zuzarte, A. Borgida, T.T. Wang, T. Li, O. Kis, Z. Zhao, A. Spreafico, T.D.S. Medina, Y. Wang, D. Roulois, I. Ettayebi, Z. Chen, S. Chow, T. Murphy, A. Arruda, G.M. O'Kane, J. Liu, M. Mansour, J.D. McPherson, C. O'Brien, N. Leighl, P.L. Bedard, N. Fleshner, G. Liu, M.D. Minden, S. Gallinger, A. Goldenberg, T.J. Pugh, M.M. Hoffman, S.V. Bratman, R.J. Hung, D.D. De Carvalho, Sensitive tumour detection and classification using plasma cell-free DNA methylomes, Nature 563 (2018) 579–583.
[57] R.A. Hlady, X. Zhao, X. Pan, J.D. Yang, F. Ahmed, S.O. Antwi, N.H. Giama, T. Patel, L.R. Roberts, C. Liu, K.D. Robertson, Genome-wide discovery and validation of diagnostic DNA methylation-based biomarkers for hepatocellular cancer detection in circulating cell free DNA, Theranostics 9 (2019) 7239–7250.
[58] L. Sigalotti, S. Coral, M. Altomonte, L. Natali, G. Gaudino, P. Cacciotti, R. Libener, F. Colizzi, G. Vianale, F. Martini, M. Tognon, A. Jungbluth, J. Cebon, E. Maraskovsky, L. Mutti, M. Maio, Cancer testis antigens expression in mesothelioma: role of DNA methylation and bioimmunotherapeutic implications, Br. J. Canc. 86 (2002) 979–982.
[59] S. Leclercq, F. Gueugnon, B. Boutin, F. Guillot, C. Blanquart, A. Rogel, M. Padieu, D. Pouliquen, J.F. Fonteneau, M. Gregoire, A 5-aza-2'-deoxycytidine/valproate combination induces cytotoxic T-cell response against mesothelioma, Eur. Respir. J. 38 (2011) 1105–1116.

[60] D.S. Schrump, M.R. Fischette, D.M. Nguyen, M. Zhao, X. Li, T.F. Kunst, A. Hancox, J.A. Hong, G.A. Chen, V. Pishchik, W.D. Figg, A.J. Murgo, S.M. Steinberg, Phase I study of decitabine-mediated gene expression in patients with cancers involving the lungs, esophagus, or pleura, Clin. Canc. Res. 12 (2006) 5777–5785.
[61] A. Kapusta, Z. Kronenberg, V.J. Lynch, X. Zhuo, L. Ramsay, G. Bourque, M. Yandell, C. Feschotte, Transposable elements are major contributors to the origin, diversification, and regulation of vertebrate long noncoding RNAs, PLoS Genet. 9 (2013), e1003470.
[62] X. Lu, F. Sachs, L. Ramsay, P.E. Jacques, J. Goke, G. Bourque, H.H. Ng, The retrovirus HERVH is a long noncoding RNA required for human embryonic stem cell identity, Nat. Struct. Mol. Biol. 21 (2014) 423–425.
[63] J. Wang, G. Xie, M. Singh, A.T. Ghanbarian, T. Rasko, A. Szvetnik, H. Cai, D. Besser, A. Prigione, N.V. Fuchs, G.G. Schumann, W. Chen, M.C. Lorincz, Z. Ivics, L.D. Hurst, Z. Izsvak, Primate-specific endogenous retrovirus-driven transcription defines naive-like stem cells, Nature 516 (2014) 405–409.
[64] D.H. Sterman, A. Recio, A.R. Haas, A. Vachani, S.I. Katz, C.T. Gillespie, G. Cheng, J. Sun, E. Moon, L. Pereira, X. Wang, D.F. Heitjan, L. Litzky, C.H. June, R. H. Vonderheide, R.G. Carroll, S.M. Albelda, A phase I trial of repeated intrapleural adenoviral-mediated interferon-beta gene transfer for mesothelioma and metastatic pleural effusions, Mol. Ther. 18 (2010) 852–860.
[65] B. Vanbervliet-Defrance, T. Delaunay, T. Daunizeau, V. Kepenekian, O. Glehen, K. Weber, Y. Estornes, A. Ziverec, L. Djemal, M. Delphin, S. Lantuejoul, G. Passot, M. Gregoire, O. Micheau, C. Blanquart, T. Renno, J.F. Fonteneau, S. Lebecque, K. Mahtouk, Cisplatin unleashes Toll-like receptor 3-mediated apoptosis through the downregulation of c-FLIP in malignant mesothelioma, Canc. Lett. 472 (2020) 29–39.
[66] C. Achard, N. Boisgerault, T. Delaunay, D. Roulois, S. Nedellec, P.J. Royer, M. Pain, C. Combredet, M. Mesel-Lemoine, L. Cellerin, A. Magnan, F. Tangy, M. Gregoire, J. F. Fonteneau, Sensitivity of human pleural mesothelioma to oncolytic measles virus depends on defects of the type I interferon response, Oncotarget 6 (2015) 44892–44904.
[67] D. Wolfe, S. Dudek, M.D. Ritchie, S.A. Pendergrass, Visualizing genomic information across chromosomes with PhenoGram, BioData Min. 6 (2013) 18.